Low Fidelity Modelling of the Nonlinear Aerodynamics of Spoilers

Alessandro Pontillo *, Punsara D.B. Navaratna †, Mark H. Lowenberg ‡,Djamel Rezgui §, Jonathan E. Cooper ¶ and Simon A. Neild ‖
University of Bristol, Bristol, BS8 1TR, UK

Spoilers are secondary control surfaces mainly used for roll control, load alleviation and as airbrakes. However, when considering very flexible wings, spoilers could also play a primary role in controlling the aircraft's attitude as an ideal alternative or complement to ailerons since they are distributed over the wingspan and, therefore, potentially less affected by the wing deformation. However, due to its nonlinear nature, spoilers aerodynamics can only be accurately simulated through high-fidelity software, such as CFD. The work presented in this paper aims to provide a novel method to model spoiler aerodynamics in a low-fidelity Unsteady Vortex Lattice framework by proposing an approach able to predict the impact of multiple spoilers on the wing lift distribution. The approach is verified through data acquired in a series of wind tunnel tests on a rigid wing equipped with servo-controlled spoilers carried out in the University of Bristol Low Turbulence Wind Tunnel. Load cell measurements and PIV data are shown for comparison. Numerical predictions show good agreement with the experimental data proving the low-fidelity UVLM aerodynamic solver's ability to successfully model the nonlinear flow field behind the extended spoiler.

Nomenclature

α	=	Angle of attack [deg]
δ_s	=	Spoiler deflection [deg]
Φ	=	Velocity potential
Γ	=	Vortex strength
AR	=	Aspect Ratio
c	=	chord [m]
C_L	=	lift coefficient
d	=	distance of spoiler collocation points from the spoiler edge
s	=	span [m]
S	=	Spoiler area [m^2]
S_n	=	Panel area [m^2]
AIC	=	Aerodynamic Coefficient Matrix
LR	=	Spoiler Left
LM	=	Spoiler Left Middle
RM	=	Spoiler Right Middle
RR	=	Spoiler Right
$UVLM$	=	Unsteady Vortex Lattice Method
V,v	=	Velocity [m/s]

*Research Associate, Department of Aerospace Engineering, MAIAA, a.pontillo@bristol.ac.uk
†Research Associate, Department of Aerospace Engineering
‡Professor of Flight Dynamics, Department of Aerospace Engineering, SMAIAA
§Senior Lecturer, Department of Aerospace Engineering
¶RAEng Airbus Sir George White Professor of Aerospace Engineering, Department of Aerospace Engineering, FAIAA
‖Professor in Nonlinear Structural Dynamics, Department of Aerospace Engineering

I. Introduction

The constant push for the improvement of aircraft performance and the advancement of state-of-the-art technology drove the modern aircraft design to have longer and slender wings [1–3]. As a result, the extensive use of composite material and the reduction in structural weight increased the flexibility of the wing, coupling the rigid body dynamics with the structural dynamics and affecting control surfaces effectiveness [4, 5]. In this context the use of ailerons as primary control surfaces may be reconsidered. In fact, ailerons are usually placed in the outboard section of the wing, where the local large deformation could reduce the aileron effectiveness and its ability to reduce the wing root bending moment in the event of gust. As a possible alternative, spoilers could be used as primary control surfaces both for maneuvering and load alleviation benefiting from the fact that they are distributed along the span and less prone to be affected by the wing deformation.

Spoilers are traditionally considered secondary control surfaces and used for roll control, load alleviation and as air breaks[6–8]. They are usually placed on the upper surface of the wing and their deflection results in a local loss of lift, associated with increased drag. Most of the work on spoiler characterisation was done in the 1970s and 1980s as a result of the inclusion of the spoilers in the aircraft control system along with the ailerons to improve lateral-directional controllability as spoilers can be deployed at any speed [8]. Aircraft flight dynamics also benefit from the use of spoilers as they introduce proverse rather than adverse yaw and prevent the excessive excitation of the Dutch roll[9].

Due to its nonlinear nature, spoilers aerodynamics is commonly characterised by either high fidelity CFD simulations or experimental tests. Multiple studies have shown that spoilers have a large impact on the local wing unsteady pressure distribution and that their effectiveness depends on the deflection angle: the higher the angle, the higher the lift reduction. However, it was found that below a certain angle, the impact of the spoiler is negligible [6].

Several efforts were made to model numerically the spoiler aerodynamics. A study done by Costes [10] considered a 2D aerofil equipped with a spoiler and found good agreement with experimental results only for spoilers placed far from the leading edge. A semi-empirical method was suggested by Mack et al. [8] where results from lifting surface predictions were corrected using experimental results. A more common option is to model the spoiler aerodynamics interpolating experimental database, such as the one provided by ESDU [6] [7] and Wentz et al. [11].

The aim of this work is to propose a novel approach for the modelling of spoilers in low-fidelity aeroelastic models to allow rapid evaluation of the spoiler effect, with a specific focus on the aerodynamics of very flexible high aspect ratio wings. The aerodynamic code adopted for the purpose of this study is a version of the Unsteady Vortex Lattice Method (UVLM) previously derived and adapted to very flexible wings by the authors [12, 13]. The proposed methods aims to modify the local circulation distribution across the deflected spoilers and estimated by the UVLM by optimizing the velocity field applied to the aerodynamic mesh to match a value of the overall variation of the lift coefficient provided by the user. Such lift variation is evaluated a priori either numerically, experimentally or with empirical formulations.

The reminder of the paper is organised as follows: Sec. II describes the adopted aerodynamic solver, focusing on the novel algorithms proposed for the implementation of the spoiler aerodynamic. Following, Sec. III provides an overview of the load cell measurements and the Particle Image Velocimetry (PIV) data obtained during tests carried out in the university of Bristol Low Turbulence wind tunnel. Sec. IV shows a numerical application of the proposed approach while Sec. V presents the final conclusions.

II. Methodology

A. Unsteady Vortex Lattice Method

The low fidelity model adopted for this study and the modelling of the spoiler aerodynamics is the well-known Unsteady Vortex Lattice Method (UVLM) [14]. Although the more general version of this code is able to model unsteady aerodynamics, for the purpose of this study only static results are presented. The UVLM is a numerical method used to solve the three-dimensional thin lifting surface problem. For this case it is assumed that the flow is potential and irrotational, and that at each control point the following boundary condition, known as zero-normal flow, is satisfied:

$$\nabla(\mathbf{\Phi} + \mathbf{\Phi}_\infty) \cdot \mathbf{n} = 0 \tag{1}$$

where $\mathbf{\Phi}$ is the velocity potential function on the surface, $\mathbf{\Phi}_\infty$ is the freestream velocity potential and $\mathbf{n}$ is the local normal vector to the panels. Furthermore, it must be true that the induced velocity at the far field is zero and that the rate of change of circulation for any line surrounding the body and the wake is zero at any time (Kelvin's theorem), i.e.

$$\frac{d\Gamma}{dt} = 0, \qquad for \quad t > 0 \tag{2}$$

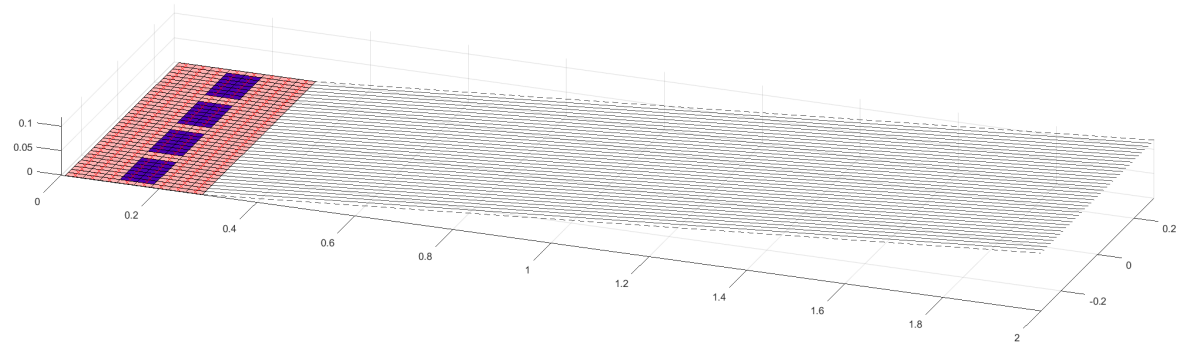

(a) Example of UVLM mesh: Rectangular wing wind tunnel model with spoilers (blue panels)

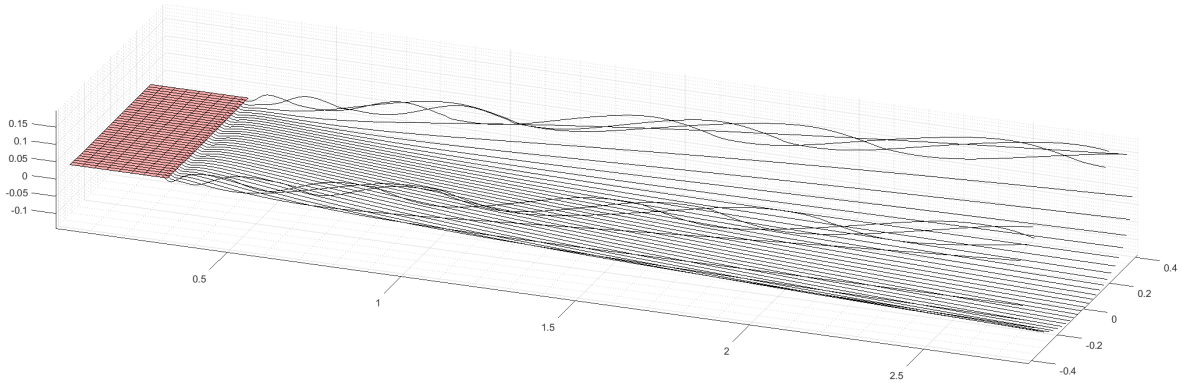

(b) Example of UVLM processing: streamlines for α = 4 deg and V = 25 m/s (no spoiler deflected)

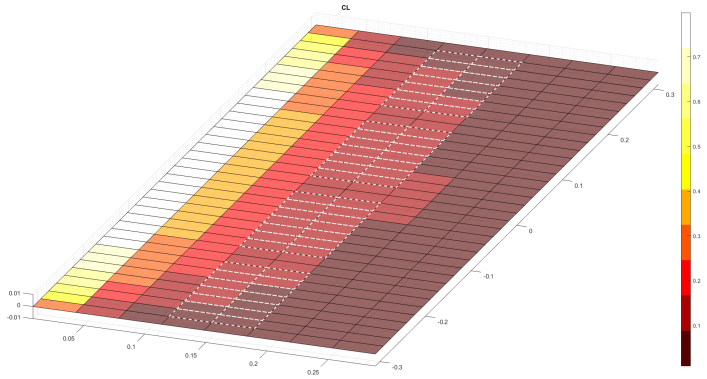

(c) Example of UVLM processing: lift coefficient panel distribution for α = 4 deg and V = 25 m/s (no spoiler deflected, spoiler panels highlighted with dashed edges)

Fig. 1 Object Oriented UVLM example. Figure (a) shows the identified spoilers along with the collocations points and the steady state free wake parallel to the leading edge local velocity vectors. Figure (b) shows some of the plotting features of the framework, displaying streamlines of the tip vortices. Figure (c) shows the ability of the framework of plotting quantities of interest along with the aerodynamic mesh.

where Γ is the circulation.

To solve the flow field and find the solution to Eq. 1-2, the approach proposed by Katz and Plotkin [14] was followed. The lifting surfaces are here divided into vortex ring elements which are made of four connected vortex filaments of vorticity γ. The boundary conditions are applied at each control point, called collocation points, which are placed at the centre of each vortex ring, on the three-quarter panel chord line. The following step is to build the Aerodynamic Coefficient Matrix, which defines the influence of each panel on the other panels of the mesh. Each element of the AIC is defined as

$$a_{nm} = [(u, v, w,)_{nm}] \cdot \mathbf{n} \tag{3}$$

where $(u, v, w,)_{nm}$ is the induced velocity of the panel m on the panel n, assuming $\Gamma = 1$. The following step is to build the Right Hand Side vector (RHS), defined as

$$RHS_i = -\mathbf{v}_i \cdot \mathbf{n}_i \tag{4}$$

where $\mathbf{v}_i$ is the velocity at the collocation point i. Finally, once AIC and RHS are computed, imposing the zero normal flow boundary condition at each collocation point results in the set of linear algebraic equations. It is important to notice, however, that differently from the original method, here the velocity at each panel is not considered constant and equal to the free stream velocity, but depends on flight conditions and the presence of high lift devices or control surfaces, like spoilers or ailerons. The set of algebraic equations to solve is defined as

$$\begin{bmatrix} a_{11} & a_{12} & \dots & a_{1n} \\ \vdots & & \ddots & \\ a_{n1} & a_{n2} & \dots & a_{nn} \end{bmatrix} \begin{bmatrix} \Gamma_{11} \\ \vdots \\ \Gamma_{nn} \end{bmatrix} = \begin{bmatrix} RHS_1 \\ \vdots \\ RHS_n \end{bmatrix} \tag{5}$$

where the vortex strenght at each panel, Γ_i can be found with standard algebraic solution methods. To find forces and moments acting on the body, different methods are possible, to resolve the aerodynamic force either in wind or body axis. However, as the work presented in this manuscript focused on the variation in lift due to the deflection of one or more spoilers, again the approach suggested by Katz and Plotking was used. In this case, the lift at each panel is found as

$$\Delta L_{nm} = \rho V_{freestream} \left(\Gamma_{nm} - \Gamma_{n-1,m}\right) \Delta y_{nm} \tag{6}$$

if the panel is not at the leading edge, or

$$\Delta L_{nm} = \rho V_{freestream} \Gamma_{nm} \Delta y_{nm} \tag{7}$$

if the panel is at the leading edge, where ρ is the density and δy is the width of the panel. The lift coefficient at each panel is defined as

$$\Delta C_{L_{nm}} = \frac{\Delta L_{nm}}{\frac{1}{2}\rho V^2_{freestream} S_{nm}} \tag{8}$$

This code was developed in an object oriented environment to make it versatile and easy to update with new additions, such as the ability to model spoilers. Specifically, the code was tailored to model and predict the aerodynamics of very flexible high aspect ratio wings with the final goal to be implemented into an aeroelastic framework [12, 13]. Figure 1 shows an example of the different features of the code. In particular, Fig. 1a shows the identification of the spoilers on the aerodynamic mesh.

B. Nonlinear spoiler aerodynamics implementation

The proposed method for the low-order spoiler modelling consists of two core parts: 1) Estimating the overall ΔC_L contribution of each spoiler due to its deflection and 2) To modify the RHS terms in Eq. 5 to distribute the contribution locally to the spoiler.

To estimate the overall loss of lift caused by the spoiler deflection multiple and different approaches can be used. The value can be tabulated as a result of experimental tests or high fidelity simulations. Furthermore, ΔC_L can also be derived either from numerical or empirical methods, such as the ESDU 14004 [6]. The evaluation of the overall ΔC_L is not within the scope of this work. For the purpose of this manuscript, the ΔC_L value is derived for a rectangular low-aspect ratio wing model through a series of wind tunnel tests, as described in Section III.

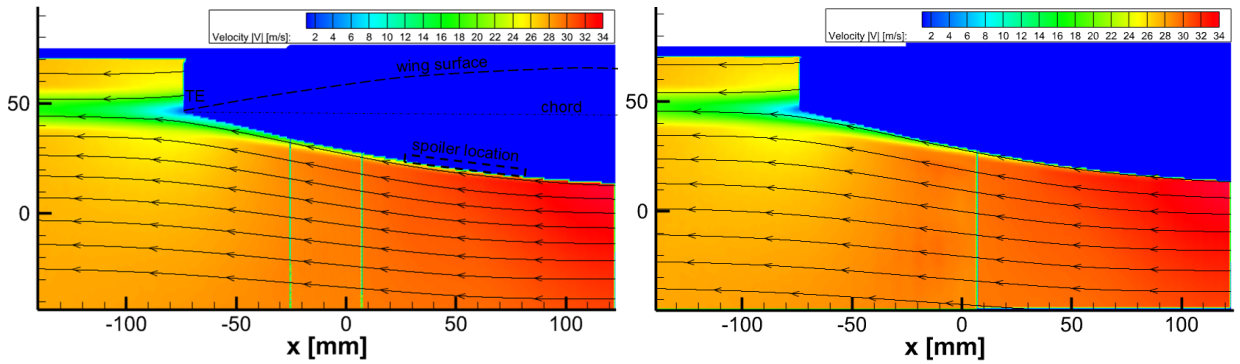

(a) Sec (1), L = 0 deg, LM = 0 deg, RM = 0 deg, R = 0deg

(b) Sec (2), L = 0 deg, LM = 0 deg, RM = 0 deg, R = 0 deg

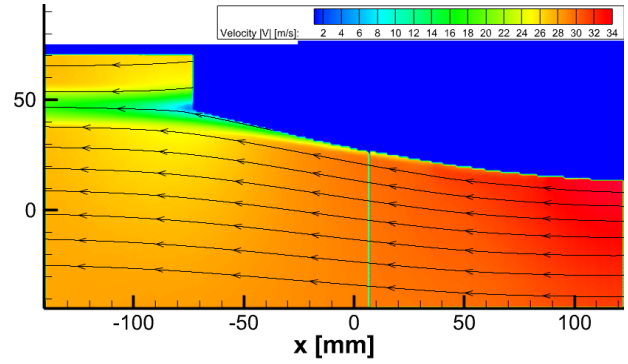

(c) Sec (3), L = 0 deg, LM = 0 deg, RM = 0 deg, R = 0deg

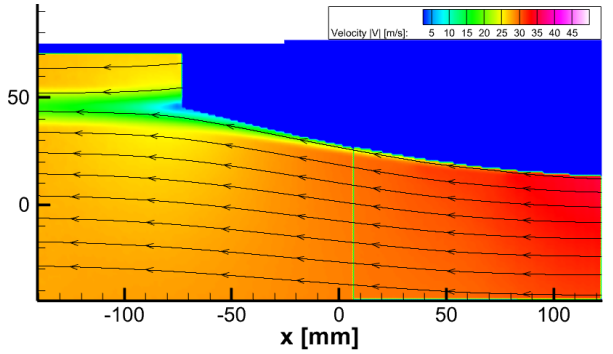

(d) Sec (4), L = 0 deg, LM = 0 deg, RM = 0 deg, R = 0deg

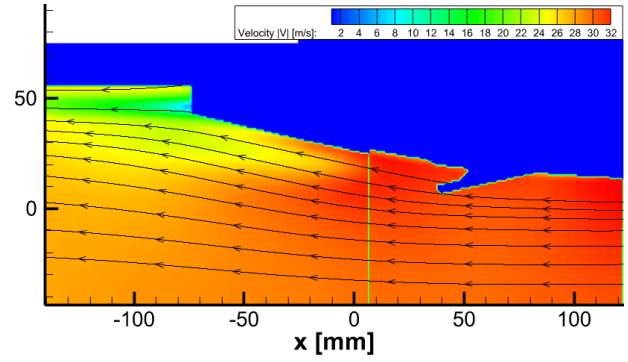

(e) Sec (1), L = 0 deg, LM = 20 deg, RM = 0 deg, R = 0deg

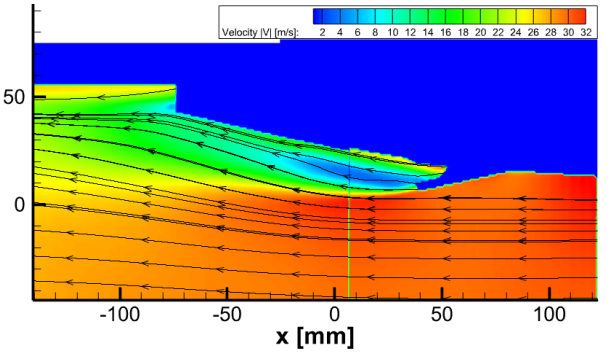

(f) Sec (2), L = 0 deg, LM = 20 deg, RM = 20 deg, R = 0deg

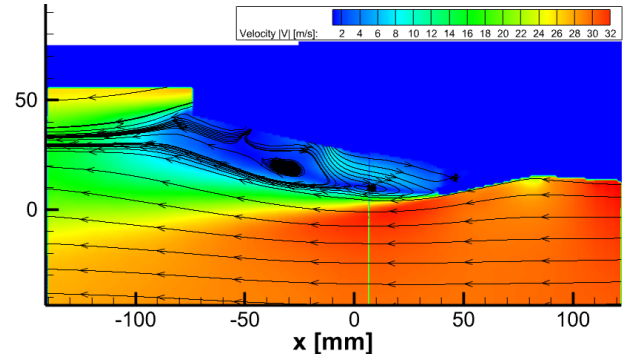

(g) Sec (3), L = 0 deg, LM = 20 deg, RM = 0 deg, R = 0deg

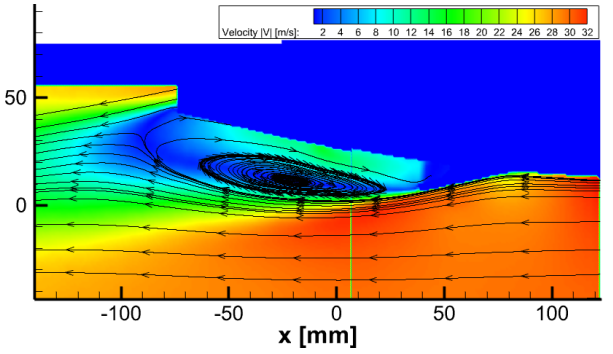

(h) Sec (4), L = 0 deg, LM = 20 deg, RM = 0 deg, R = 0deg

Fig. 2 PIV results to compare baseline case (no spoiler) with LM=20 deg spoiler deflected ($\alpha = 0$, v=25 m/s). In the figures, the wing is shown upside down (testing position) and the blue area identifies the masked area, the region where the PIV particles could not be lit by the laser sheet. Figure (a) shows the boundaries of the aerofoil and the position of the spoiler.

Once the overall ΔC_L is estimated, the following step is to distribute its effect locally on the aerodynamic mesh. As the aerodynamic force distribution depends on the velocity field applied to the collocation points, to account for the spoiler deflection it is suggested that the terms $RHS_i = -\mathbf{v}.\mathbf{n}$ within Eq. 5 be modified, i.e. tailor the local velocity field. The optimized velocity distribution is used to generate the new solution $\mathbf{\Gamma}$ that produces the new aerodynamic force distribution, according to Eq 6-8. In the proposed method, the local velocity field is optimized such that the overall variation of lift coefficient, due to the newly evaluated vortex strength field $\mathbf{\Gamma}$, with respect to a clean no-spoiler configuration, converges to user-defined C_L^{target}, as described in Algorithms 1-2.

For the scope of this paper, different assumptions were made in the estimation of the optimized velocity field:

- The velocity change in the optimization process is imposed only at the collocation points included in the area behind the spoiler within the wing trailing edge, spoiler trailing edge and the projection of the spoiler edges. This assumption is based on experimental observation as result of PIV tests run on the rigid model wing where it was noticed that the spoiler effect is mostly confined to the region behind the spoiler in the flow direction. More details can be found in Section III.B.
- Only the magnitude of the velocity is optimized using a scale factor that impacts the three components of the velocity *(u,v,w)* in the same way. The result is that the optimized velocity will be applied along the same direction of the original one.
- The same variation of the velocity field is applied to all spoilers in the event multiple spoilers are deflected. This assumption was made to simplify the numerical algorithm and eliminates the need to apply different weights to different spoilers in their contribution to the overall ΔC_L. Relaxing this limitation is the subject of future work.
- The algorithm does not run any check on the value ΔC_L, which is externally provided by user.
- The effect of multiple spoilers is modelled as the linear combination of the effect of each individual spoiler - justified by evidence collected during the experimental campaign.

Based on experimental observations, the drop in the velocity field at each row of panels behind the spoiler was model by implementing the following smooth function

$$f(x) = \begin{cases} x(2)|1 - x(1)|\frac{\exp^{\frac{1}{d}}}{\exp^{\frac{1}{d}} + \exp^{\frac{1}{1-d}}} + x(1), & \text{if } 0 \leq d \leq 1 \\ x(1)x(2), & \text{otherwise} \end{cases} \tag{9}$$

where d is the distance of the collocation point from the spoiler edge and f is a function of the parameters *x(1)* and *x(2)*. These two parameters constitute the vector $\mathbf{x} = [x(1), x(2)]$, which is the optimized state in the optimization algorithm. A general trend of Eq. 9 is shown in Fig. 3, for $\mathbf{x} = [0.9, 0.8]$. Fig. 2 shows experimental evidence to justify the adoption of Eq. 9. The top four plots show velocity magnitude and streamlines at four different spanwise locations across the spoiler (as defined in Fig. 10) for the clean configuration, i.e. no spoiler deflected. As expected, the velocity field is constant across the spoiler length. The bottom four plots show the same four sections across the spoiler deflected to $\delta_s = 20$ deg. At section 1, just after the spoiler edge, the effect of the spoiler is already evident with a local drop of velocity (yellow bubble) that is not present at the same section of the clean case. At the edge of the spoiler (section 2), the flow is not reversed yet, but the drop of velocity is already large. Moving further towards the spoiler centre, a re-circulation bubble is generated, to be fully developed at the mid spoiler location (section 4), where a reversed velocity flow field is evident.

The solving algorithm is described in Algorithm 1, while the adopted cost function for the optimization process is described in Algorithm 2. As already mentioned, the adopted UVLM code is built as object oriented. The algorithm starts by initialising two objects, one UVLM object that contains the lifting surface properties, such as geometry, wake and vortex rings, and the velocity field characteristics. A second object is created from a different class, that contains the spoiler properties, i.e. geometry and deflection angles. After the two objects are created, the algorithm estimates a first baseline solution, i.e. without the contribution of the spoilers. This generates a baseline value of the lift coefficient, C_L^{TOT} that is used in the objective function. After this, once the ΔC_L is defined by the user, the algorithm starts the optimization routine. The optimization variable is the vector $\mathbf{x}$ that defines the smooth function (Eq. 9). In the objective function, after guessing the value of $\mathbf{x}$, the smooth function trend is evaluated. The smooth function represents the drop in velocity across the spoiler from the edge to the mid section. The second half of the velocity profile is then mirrored with respect to the spoiler centreline. The following step is to interpolate the drop in velocity at each of the identified collocation points behind the spoiler as a function of their distance from the spoiler edge, d, i.e.

$$v_{drop}(d) = f(x, d) \tag{10}$$

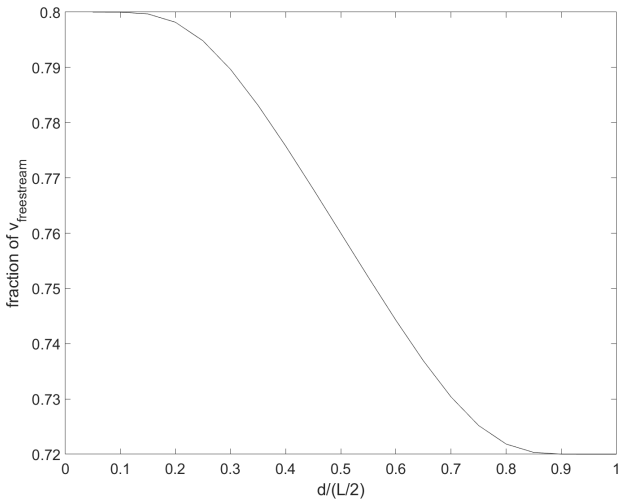

Fig. 3 Example of smooth function used in the optimization algorithm [x(1) = 0.9, x(2) = 0.8]

Algorithm 1 Object Oriented UVLM code including the modelling of the nonlinear aerodynamics of spoilers

Initialise *UVLM object*
Import mesh and define lifting surfaces properties
Initialise *Spoiler object* subclass of *UVLM object* ▷ constructor: inner edge, outer edge, chord, length, hinge distance from leading edge
Define $v_{freestream}$ field at each collocation point
Calculate AIC
Baseline solution **AIC** $\Gamma = -\mathbf{v}_{freestream} \cdot \mathbf{n}$
Calculate C_L panels as $C_L^i = \frac{L^i}{0.5\rho|v_{freestream}|^2 S^i}$
Calculate overall C_L^{TOT} baseline
Define target ΔC_L due to spoiler(s) deflection ▷ Empirical data, numerical data, experimental datasets
while $C_L^{opt} - (C_L^{baseline} - \Delta C_L^{target}) \neq 0$ **do**
    run *constrained f min algorithm* on objective_function(@($\mathbf{x}, \mathbf{x_0}$)) with $0 \leq \mathbf{x} < 1$
end while

The new velocity distribution is applied at each collocation point behind the spoiler, in the row-wise direction, for all panel rows within the wing trailing edge and the spoiler trailing edge. The new velocity field, $\mathbf{v}_i$, is then used to evaluate the new $\mathbf{\Gamma}$ solution solving Eq. 5, where the new *RHS* is defined using the new velocity field as $RHS_i = -\mathbf{v}_i \cdot \mathbf{n}$. The new vorticity solution defines the new C_L^{TOT}, which is used to evaluate the cost function, *cf*

$$cf = C_{L_i}^{TOT} - C_L^{target} \tag{11}$$

where

$$C_L^{target} = C_{L_{baseline}}^{TOT} - \Delta C_L \tag{12}$$

Fig. 4 shows an example of the spoiler modelling applied to the low-aspect ratio wing described in Section III. On the left-hand side of the figure results for a requested $\Delta C_L = 0.095$ are presented. In this case the required ΔC_L represents a drop of 50% in the wing lift and just one spoiler is deployed. The top figure shows the C_L distribution across the wing, where the drop in C_L is clear behind the spoiler. In this region a local negative of the lift coefficient indicates a reverse flow. The effect of the spoiler is also reflected in the wake, as shown in the streamline plot. Finally, the bottom plot shows the lift distribution with and without the spoiler deflected. On the right-hand side, a similar situation is proposed, where a $\Delta C_L = 0.13$ (70% drop) is requested by deflecting all four spoilers. In this case the effect of the spoilers extends to the wholw wing, with the entire trailing edge stalled (reversed flow).

Finally, Fig. 5 shows the impact of the x(2) parameter on the solution of the flow field behind the spoiler. Initially the parameter was constrained to be strictly positive. However, it was noticed that the ability of the code to model higher

Algorithm 2 Objective function

1: Evaluate Eq. 9 for the initial value $\mathbf{x}_0$ (i=1) or the i-th iteration value $\mathbf{x}$
2: Calculate the percentage drop in velocity at the spoiler aft nodes as function of the distance d from the spoiler edge
3: Update the velocity field by substituting the value of the $\mathbf{v}_{freestream}$ with the newly calculated velocity at the spoiler aft nodes $\rightarrow$ new velocity field $\mathbf{v}_i$
4: Evaluate the new solution **AIC** $\Gamma_i = -\mathbf{v_i} \cdot \mathbf{n}$
5: Evaluate the new $C_{L_i}^{TOT}$
6: Evaluate $C_{L_i}^{TOT} - C_L^{target}$

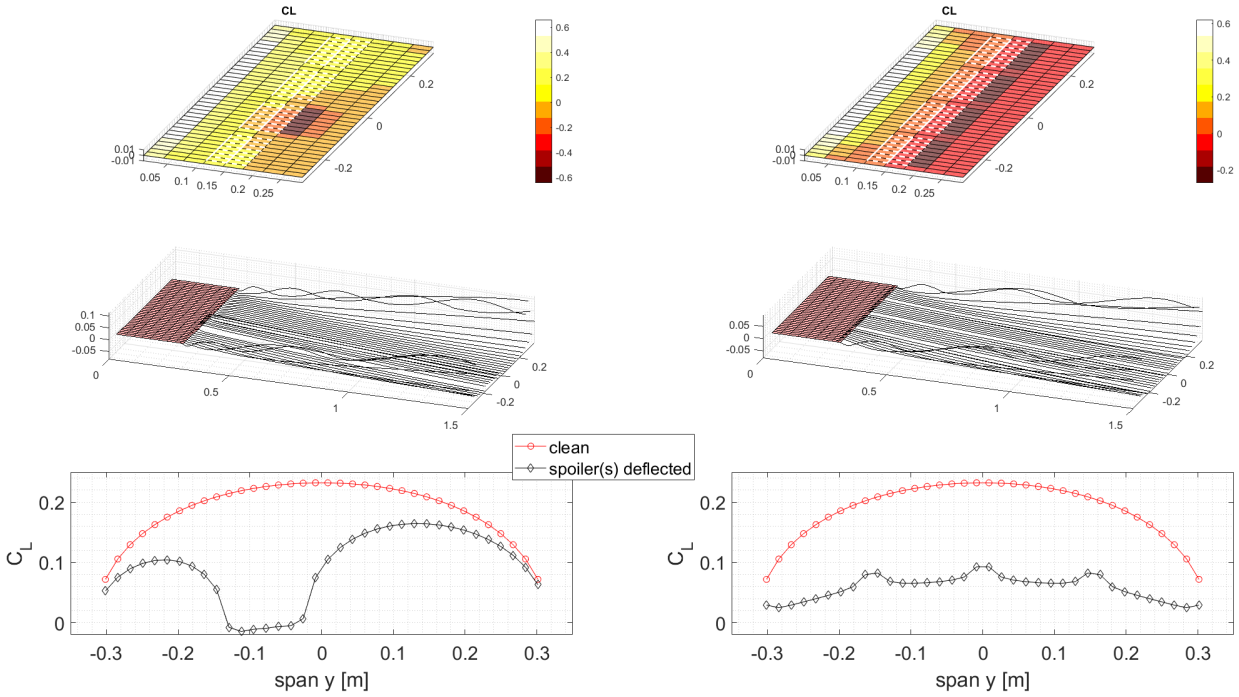

Fig. 4 Example of spoiler deflection simulated within UVLM. Left: left middle spoiler deflected - $\Delta C_L = 0.095$ **(50%),** $C_{L_{baseline}} = 0.188$**,** $C_{L_{target}} = 0.0934$**,** $C_{L_{opt}} = 0.0934$**. Right: all spoilers deflected -** $\Delta C_L = 0.13$ **(70%),** $C_{L_{baseline}} = 0.188$**,** $C_{L_{target}} = 0.0584$**,** $C_{L_{opt}} = 0.0584$

values of ΔC_L was limited by such a constraint as if $x(2) > 0$ the flow cannot be modelled as reversed. On the left-hand side of Fig. 5, it can be seen that the optimizer is able to match C_L^{target} until x(2) = 0, when the velocity field behind the spoiler is zero at each collocation point. By relaxing the constraint on the lower boundary of x(2) (right-hand side plots), the optimizer is now able to model a reversed velocity flow field, which provides the required local ΔC_L to match the overall loss of lift coefficient.

III. Experimental setup and results

The aim of the wind tunnel tests was to gather enough data 1) to verify the modelling of the spoiler into UVLM, and 2) to characterise the flow behind the spoiler in order to select the most appropriate velocity function to model the spoiler's induced velocity field. For the purpose of these experimental tests, a low aspect ratio wing rigid model was used to avoid wing deformation in order to limit the factors that could interfere with the assessment of the spoiler aerodynamics. The model CAD is shown in Fig. 6. The model is made of four 3D printed sections (ABS), assembled on two steel rods. The model is equipped with four servo-controlled spoilers, one servo-controlled leading edge slat and one servo-controlled aileron, although for the purpose of this work, the slat was always retracted and the aileron not deflected (i.e. $\delta_a = 0$), while only the two middle spoilers were employed for the tests. The wing aerofoil is the symmetric NACA 0021, the wing chord is $c = 0.28$ m, the span is $b = 0.62$ m, for an aspect ratio $AR = 2.1$. The wing is

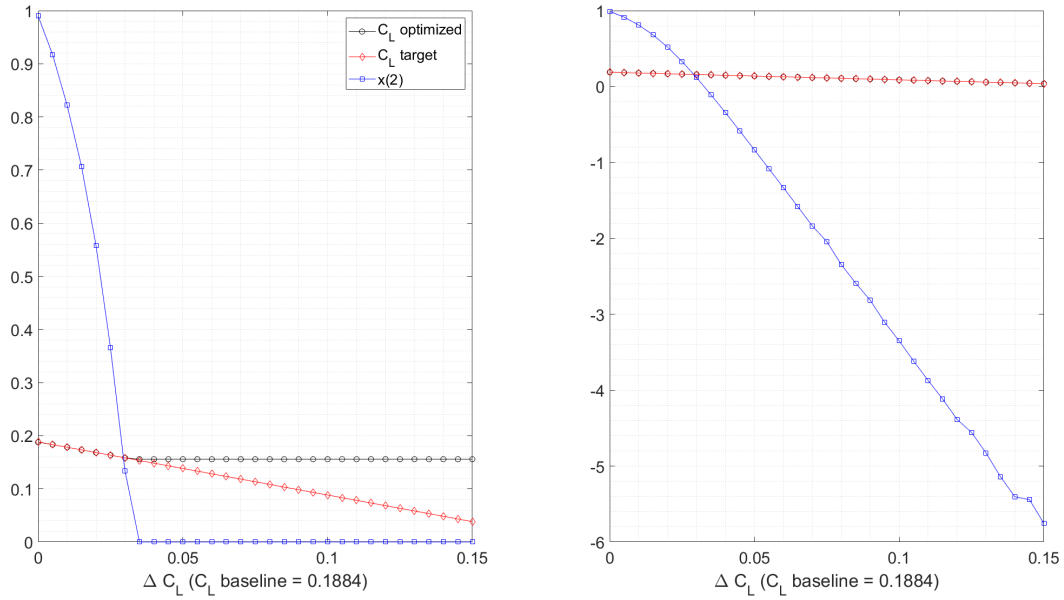

(a) Impact of parameter x_2 on the max ΔC_L achievable. Left; $x_2 \in [0, 1)$. Right: $x_2 \in [-\infty, 1)$

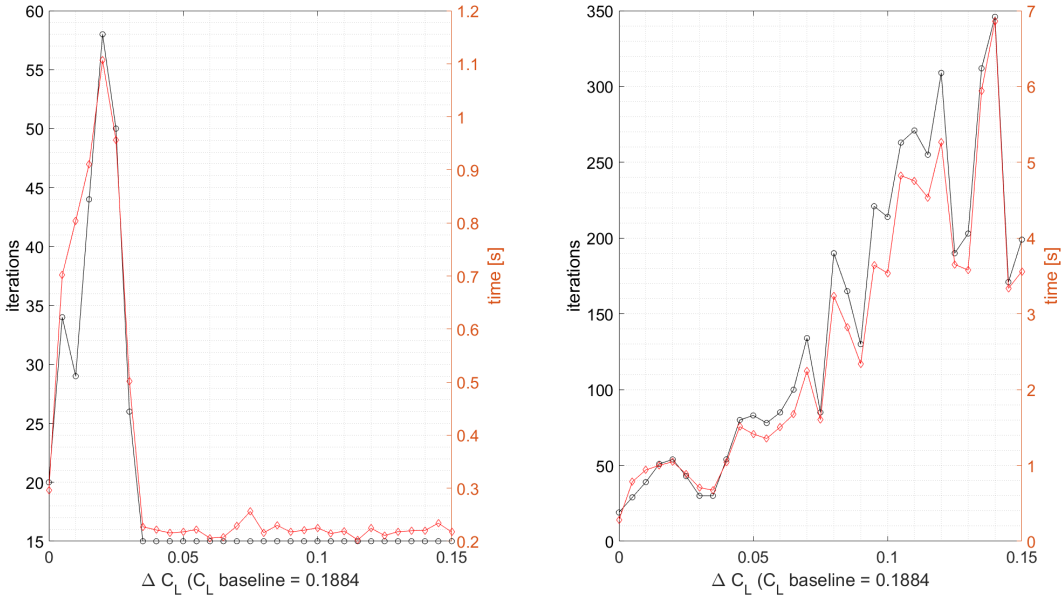

(b) Impact of parameter x_2 on the number of iterations and computational time. Left; $x_2 \in [0, 1)$, Right: $x_2 \in [-\infty, 1)$.

Fig. 5 Impact of parameter x_2 on the modelling of spoiler aerodynamics ($\alpha = 4$ deg, v = 25 m/s).

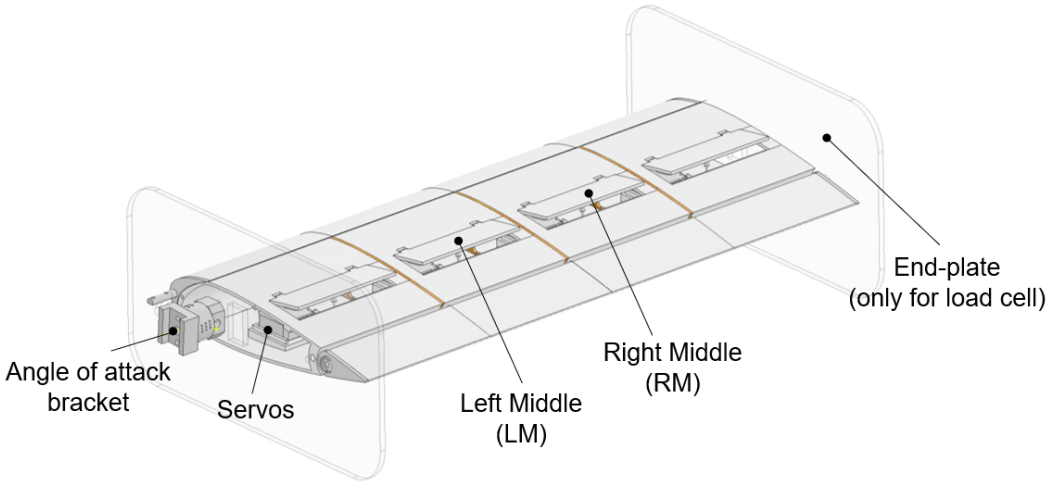

(a) Model wing CAD with components. From left to right, spoilers are identified, where the two adopted spoiler for the test were the Left Middle (LM) and the Right Middle (RM) spoilers.

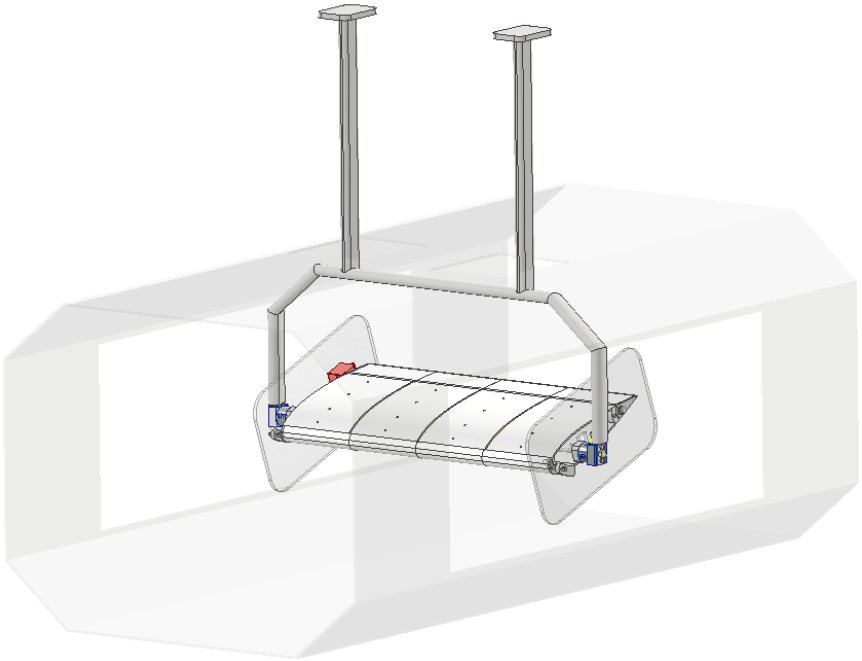

(b) CAD of the wind tunnel with the model mounted at positive angle of attack. The figure shows the wing model in the load cell configuration (with end-plates)

Fig. 6 CAD of rigid wing model adopted for the wind tunnel test campaign

straight (taper ratio $\lambda = 0$), with no sweep. The wing model is connected to the load cell bracket (Fig. 6b) through a mechanical angle of attack mechanism able to provide a range of incidence $-28\ deg \leq \alpha \leq 28\ deg$. Two end-plates were used for the load cell measurements to prevent 3D tip effects, while end-plates were not used for PIV measurements to prevent distortion in the camera readings. The model was tested in the University of Bristol Low Turbulence wind tunnel [15] for different speeds and angles of attack. The Low Turbulence tunnel is a closed-circuit wind tunnel with a maximum speed of 100 m/s, turbulence intensity lower than 0.05% and an octagonal test section of 0.8 m x 0.6 m.

A. Load cell measurement

For the load cell measurement, the model was connected to the 3-DOF overhead balance through the U-bracket as shown in Fig. 6b. Lift and drag were estimated from the processing of the data for two sets of angle of attack (α = 6 deg and α = 14 deg) at two different speeds (v = 15 m/s - Re = $2.76 \cdot 10^5$ and v = 20 m/s - Re = $3.56 \cdot 10^5$). For each combination of (α, v), different combinations of left middle and right middle spoiler deflection were tested. Fig. 7 and 8 show the processed results, where the C_L and the ΔC_L (decrement in lift due to spoiler deflection) are reported. For both cases, results for the deflection of only one spoiler, the left middle (top left), and a combination of the left middle and right middle spoilers are presented. As expected, for the same incidence, the velocity does not impact the C_L value. For α = 6 deg, the decrement in lift coefficient due to spoiler deflection can be considered linear. For example the decrement in C_L for LM=10 and RM=10 (middle point, plot in the top-right corner) is comparable to the one for LM=20 and RM=0 (left point, plot in the bottom-right corner). This behaviour is also observed in the PIV results were the region between the LM and RM spoilers is not largely affected by the spoiler deflection. This experimental evidence justifies the application of the superposition principle in modeling the interaction between multiple spoilers. Results for α = 14 deg show a much lower spoiler efficiency than the one shown for α = 6 deg. This behaviour can be explained by the fact the aerofoil is stalled ($\alpha_s \approx 8$ deg), therefore spoilers operates in a separated flow. Nevertheless, trends for the variation of lift coefficient hold and show the same tendency of the α = 6 deg case.

B. Particle Image Velocimetry (PIV)

The flow field around and after the spoiler was measured by adopting 2D two-component PIV. The acquisition frequency for the test was f = 200 Hz for t = 5 s, for a total of 1000 frames captured for each test. Two Photon FastCAM MiniWX 100 cameras with a resolution of 2078x2078 px were used and results were processed in LaVision DaVis software. The acquisition was done at four different planes, assuming that the velocity field across the spoiler is symmetric with respect the centre line, as detailed in Tab. 1 and shown in Fig. 10. Fig. 9a shows the rigid wing model

Table 1 PIV test details

Section	distance from b/2 [m]	Note
1	0	half wing (between LM and RM)
2	0.015	LM spoiler edge
3	0.035	-
4	0.075	LM mid-section

mounted in the Low Turbulence tunnel test section, with no end-plates and the calibration screen used to calibrate the PIV system, while Fig. 9b shows a photo captured by the camera during one of the tests. Results presented in this section are for α = 0 deg and v = 25 m/s and are shown in Fig. 11. Plots show the average velocity field across the spoiler and the trailing edge (with a portion of the wake) along with streamlines for the identification of any recirculation bubble.

Fig. 11a shows the flow at the spoiler mid-section for the spoiler deflection LM = 10 deg. What it is interesting to notice in this case is that, although a recirculation bubble is present, the stall region does not extend to the trailing edge but it is limited to the region immediately behind the spoiler. This suggests that the assumption made in the modelling of the spoiler in UVLM, i.e. all the collocation points behind the spoiler are affected by the deflection, does not always hold and there is a need for further investigation on the matter. The following three plots (Fig. 11b,11c and 11d) show that the larger the deflection angle δ_s, the greater is the region affected by the spoiler and the more severe is the drop in velocity due to the flow recirculation. The reversed flow is indicated by the direction of the streamlines.

Finally, the last two plots the section in between the LM and the RM spoilers (Fig. 11e) and the LM mid-spoiler section (Fig. 11f) when both spoilers are deployed. This case was investigated to address the impact of spoilers on the adjacent ones. When comparing Fig. 11e with the clean-configuration equivalent (Fig. 2a), it can be noticed that although there is a larger area of slowed flow at the trailing edge, overall the flow between the two spoilers looks unaffected, which justify the assumption of using the superposition principle. Similarly, comparing Fig. 11f with Fig. 11b (only LM spoiler deflected) at the spoiler mid-section, the two flow fields look identical.

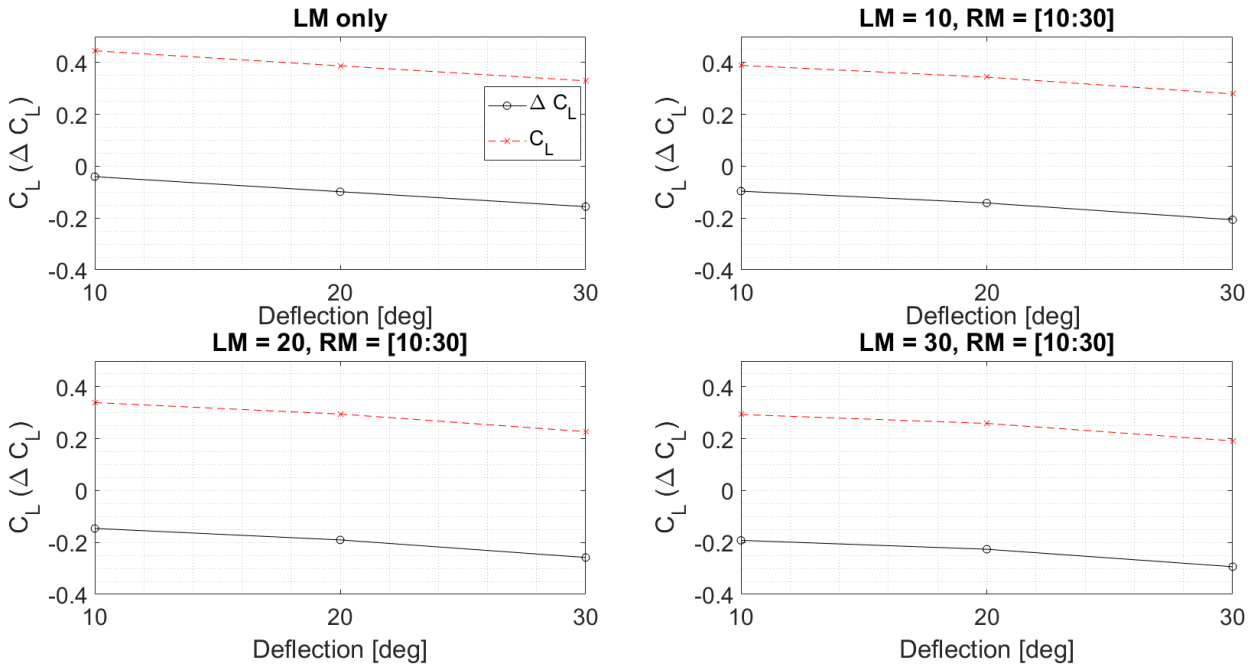

(a) v = 15 m/s

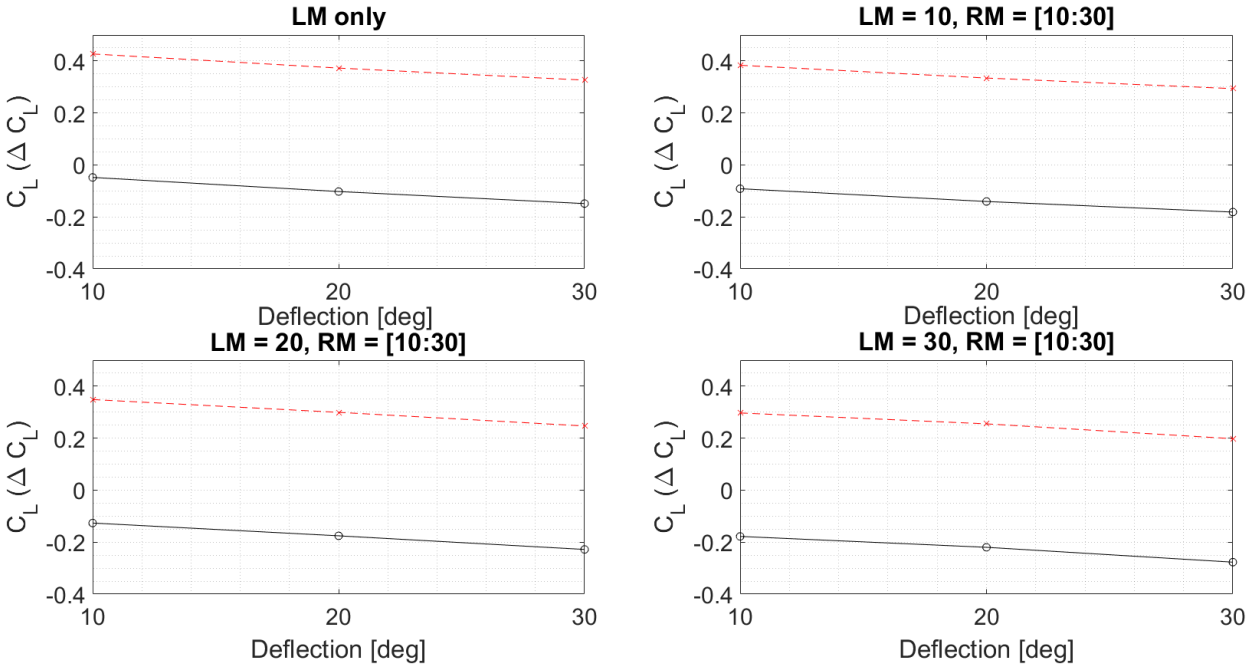

(b) v = 20 m/s

Fig. 7 Load cell data (α = 6 deg)

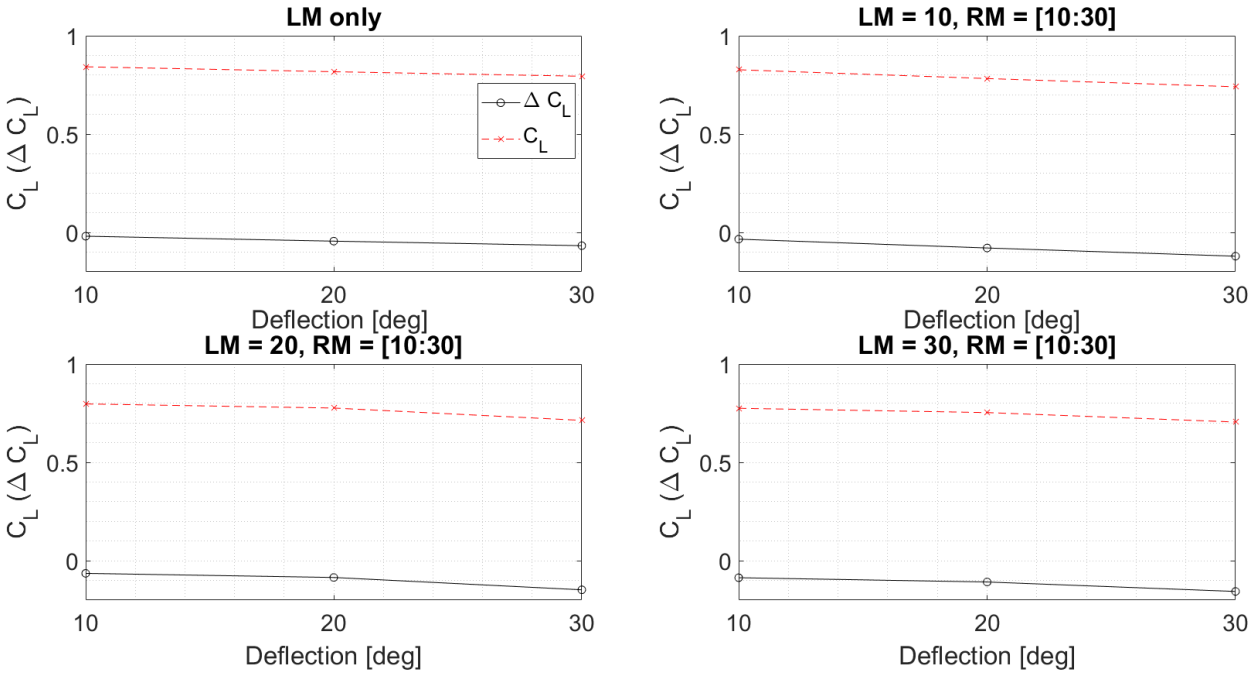

(a) v = 15 m/s

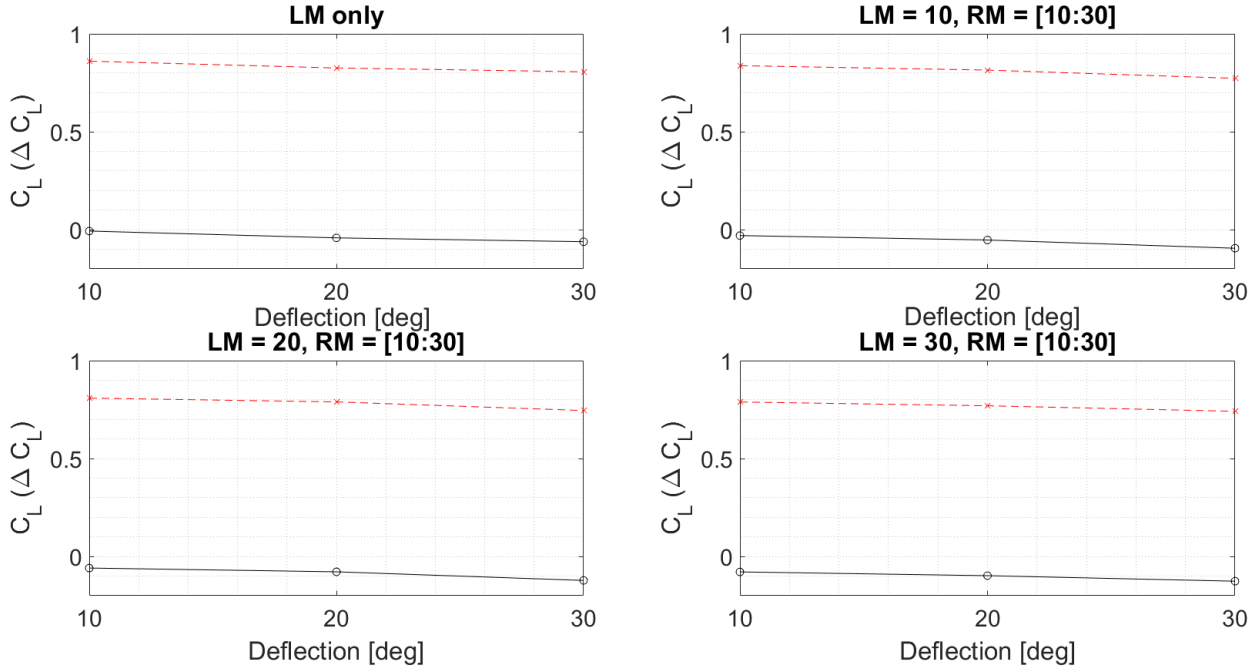

(b) v = 20 m/s

Fig. 8 Load cell data (α = 14 deg)

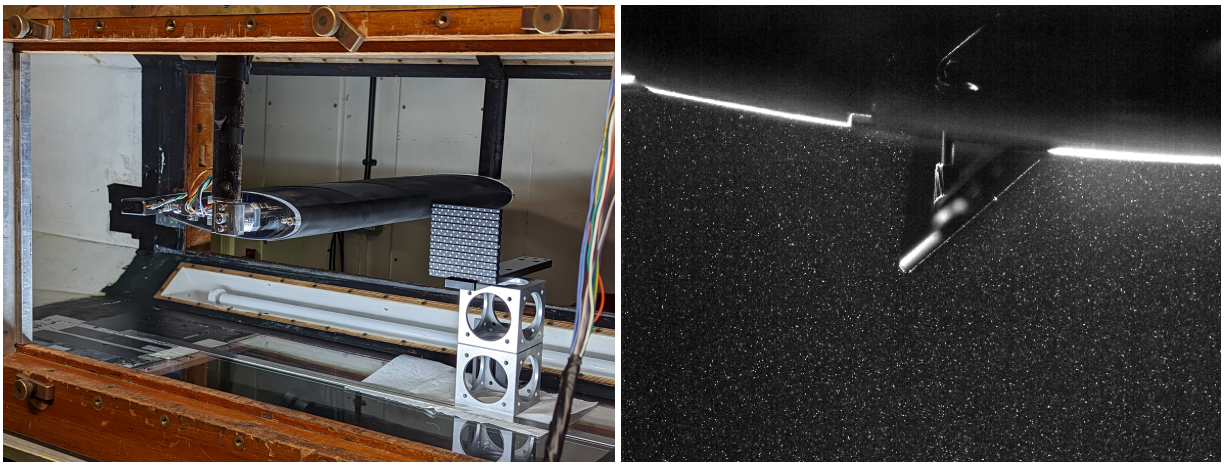

(a) The rigid wing model during the laser calibration **(b) PIV particles around the extended spoiler**

Fig. 9 PIV setup (no end-plates)

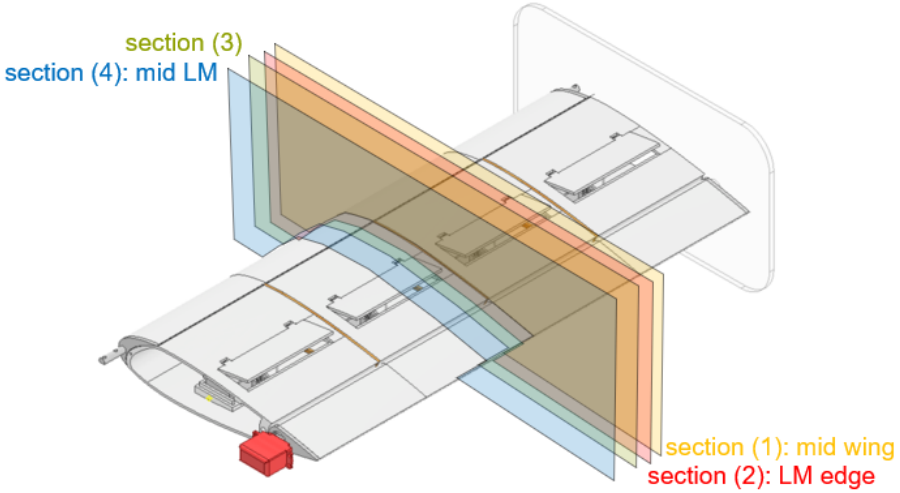

Fig. 10 Sections of the rigid wing tested within the PIV experiment

IV. Test case

In this section, an application of the low-fidelity aerodynamic code is presented to show the potential of the proposed method. The UVLM along with the spoiler modeling is used here to replicate wind tunnel results of the experiment described in Sec. III

A. Wind tunnel data

As previously mentioned, because speed does not impact the C_L trends and values for fixed angle of attack, it was decided to chose only one of the two cases and to simulate the condition for α = 6 deg and v = 15 m/s. The second case, where α = 14 deg was not simulated as typically UVLM is a linear solver, unable to predict and simulate stall. Although there are plans to extend the current UVLM to include stall prediction, it is currently not possible to simulate aerofoils beyond their stall incidence. Fig. 12 shows the simulation results. The top-left corner shows the optimized solution for the required ΔC_L achieved with the deflection of the left middle spoiler. With the help of Tab. 2 it can be seen that the single spoiler can converge to the optimal C_L without generating any recirculation bubble for δ_s = 10 deg, which is consistent with results shown by the PIV plots, where for δ_s = 10 deg, although separation was present, most of the flow

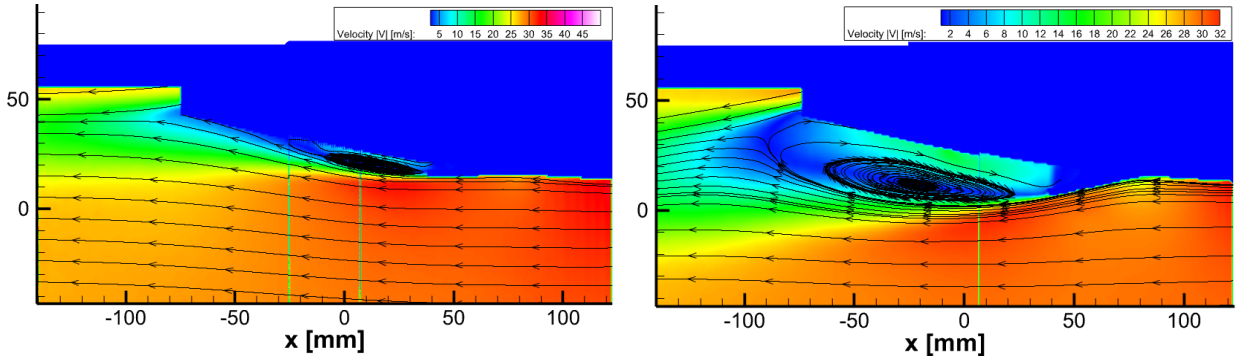

(a) Sec (4), L = 0 deg, LM = 10 deg, RM = 0 deg, R = 0deg

(b) Sec (4), L = 0 deg, LM = 20 deg, RM = 0 deg, R = 0 deg

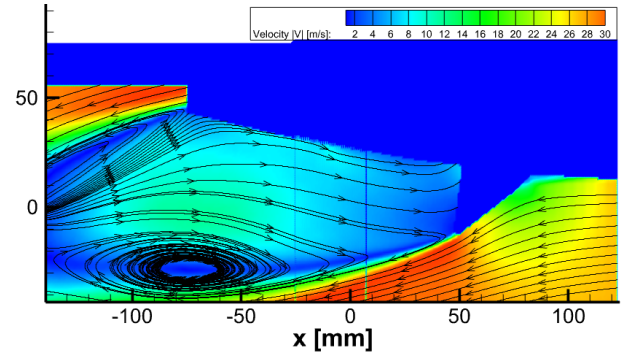

(c) Sec (4), L = 0 deg, LM = 45 deg, RM = 0 deg, R = 0deg

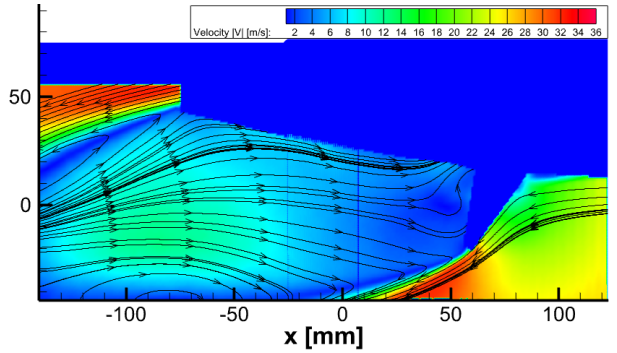

(d) Sec (4), L = 0 deg, LM = 60 deg, RM = 0 deg, R = 0deg

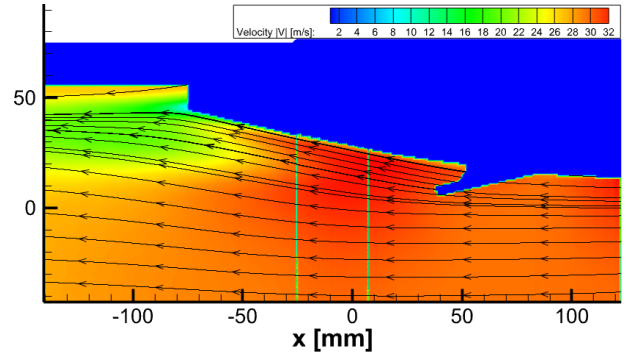

(e) Sec (1), L = 0 deg, LM = 20 deg, RM = 20 deg, R = 0deg

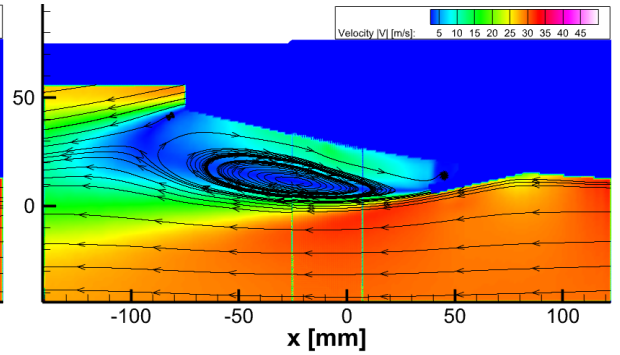

(f) Sec (4), L = 0 deg, LM = 20 deg, RM = 20 deg, R = 0deg

Fig. 11 PIV average velocity and streamlines (α = 0 deg, v = 25 m/s)

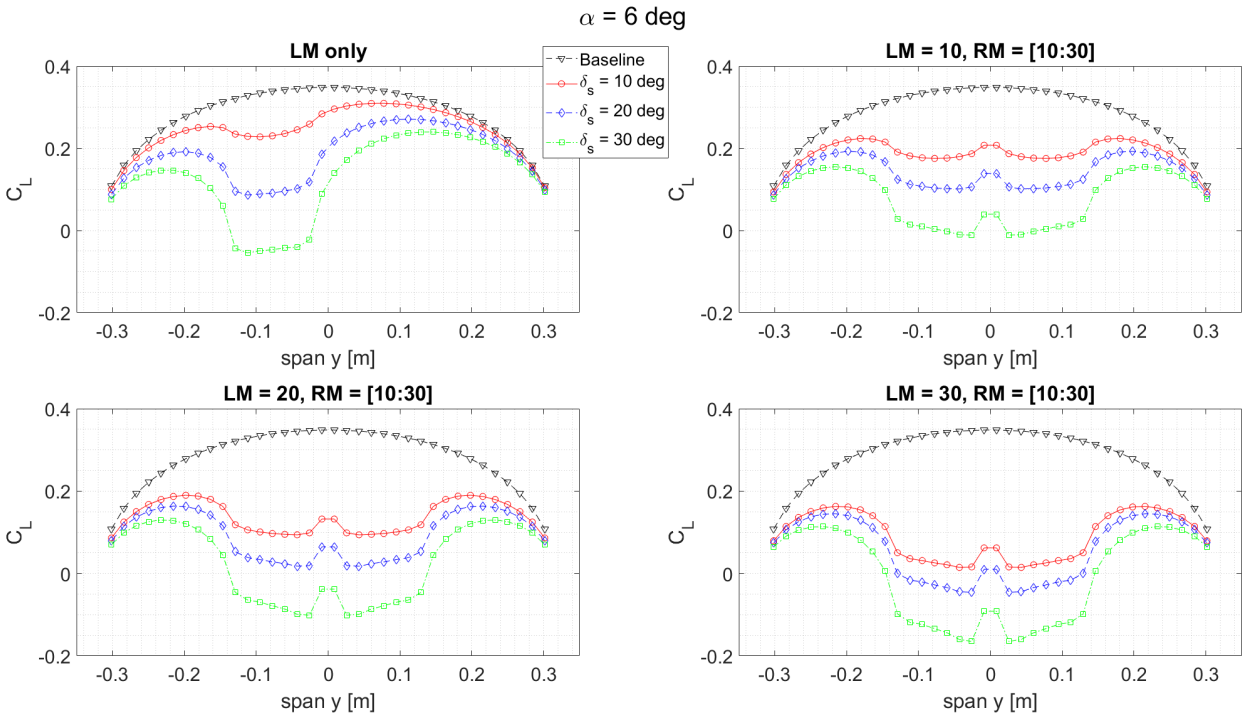

Fig. 12 Modelling of wind tunnel data as shown in Fig. 7a (α = 6 deg and v = 15 m/s)

Table 2 Algorithm performance

	ΔC_L^{WTT}	ΔC_L^{opt}	Error [%]	Opt time [s]	Iterations	Reversed flow [Y/N]
LM only	0.04	0.04	-1.9e-05	1.5	60	No
	0.10	0.10	-1.9e-05	0.7	26	Yes
	0.15	0.15	-1.9e-05	3.1	131	Yes
LM=10,RM=[10:30]	0.09	0.09	-1.9e-05	0.8	26	No
	0.14	0.14	-1.9e-05	4.1	163	Yes
	0.21	0.21	-1.9e-05	1.9	71	Yes
LM=20,RM=[10:30]	0.14	0.14	-1.9e-05	4.3	179	Yes
	0.19	0.19	-1.9e-05	4.7	193	Yes
	0.26	0.26	-1.9e-05	4.8	209	Yes
LM=30,RM=[10:30]	0.19	0.19	-1.9e-05	3.4	145	Yes
	0.23	0.23	-1.9e-05	0.6	20	Yes
	0.29	0.29	-1.9e-05	7.2	312	Yes

reattached behind the spoiler towards the trailing edge. For δ_s = 20 deg and δ_s = 30 deg the solution shows reversed flow in the region behind the spoiler and a negative local C_L for δ_s = 30 deg. The following plots show a combination of the LM and RM spoilers to achieve the required lift drop. What it is interesting to notice in these plots is that the lift distribution is always symmetric even though the left and right spoilers experience different δ_s. This is a current limitation of the software that applies the same optimized velocity distribution to each spoiler. This assumption was initially made because the deflection angle δ_s is not actually an input to the solver, but it is used to evaluate the correct ΔC_L, e.g. by interpolating look-up tables or interpreting the ESDU 14004 data sheet. To overcome this limitation, it would be necessary to increase the number of optimization parameters to $2N$, where N is the number of spoilers. This choice, while it would improve the local prediction of the local lift distribution, would also increase the number of parameters to optimize, therefore the optimization time.

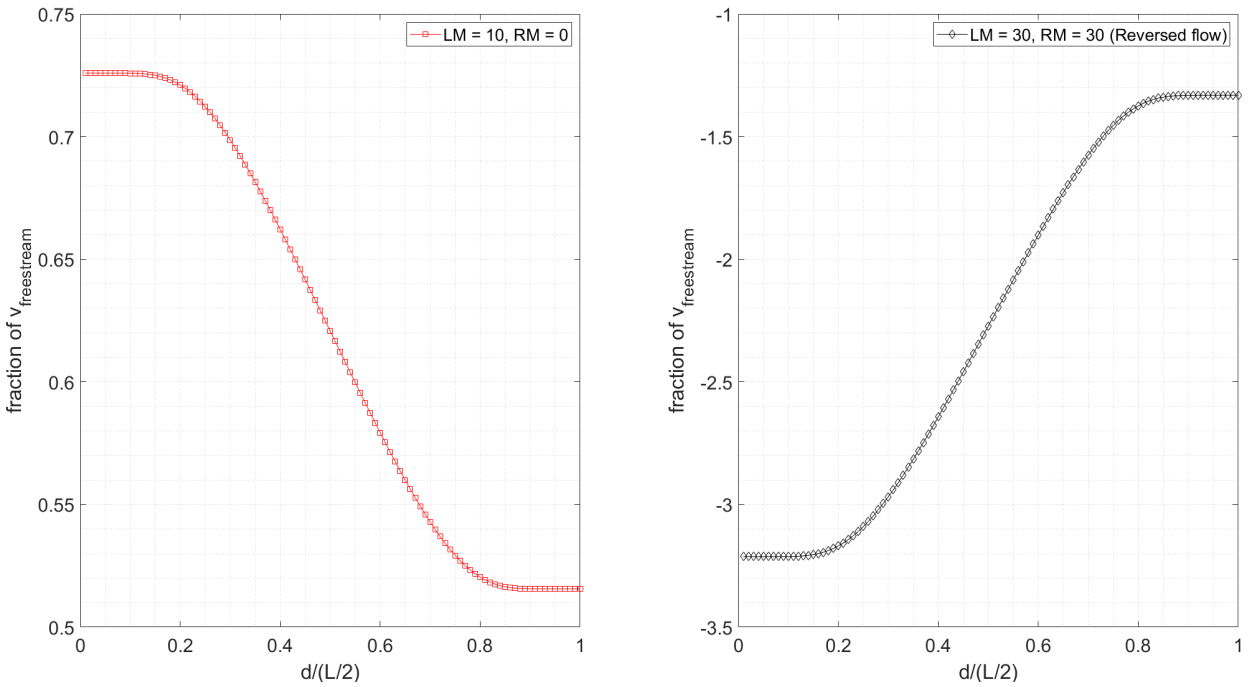

Fig. 13 Optimized velocity profile for two different solutions (Left: LM=10, RM=0, Right: LM=30, RM=30)

Tab. 2 shows the performance of the optimizer for the different cases. The optimizer was always able to converge to the target value. As a local optimizer was chosen for the task, the number of iterations and the computational time depend on the choice of the initial conditions, explaining the lack of consistency in the optimization time across the different cases. The last column shows that only in 16% of the cases did solution not present reversed flow.

Finally, Fig. 13 shows two different examples of the optimized velocity profile. The left-hand side plot shows the case when the flow is not reversed and the velocity drops from about 73% of $v_{freestream}$ at the edge to about 51% of $v_{freestream}$ at the spoiler mid-section. The right-hand side plot instead shows a typical reverse flow velocity profile, where the flow goes from about three times the freestream velocity at the edge of the spoiler (but opposite direction as negative sign) to about 1.25 times the freestream velocity at the spoiler mid-section, still in the opposite direction.

V. Conclusions

This paper proposes a novel method to model the nonlinear aerodynamics of spoilers in a low-fidelity aerodynamic framework. The framework adopted for this study was an object oriented version of the Unsteady Vortex Lattice Method (UVLM).

Experimental data derived from load cell measurements and Particle Image Velocimetry (PIV) were presented to support the numerical modeling of the spoiler within the aerodynamic framework. The principal observations from the results are: 1) there is not a strong interaction between neighbouring spoilers, therefore the adoption of the superposition principle is acceptable and 2) the modeling of reversed flow (recirculation bubbles) is necessary to predict the correct variation of lift, ΔC_L. It is however understood that the experimental campaign only considered a limited data set of possible wing geometries and that a deeper investigation is required.

With these assumptions made, the velocity field behind the spoiler was modelled through the use of a smooth function. A local optimizer was then implemented to optimize the spoilers' induced velocity profile to converge to a prescribed C_L^{target}, a function of the lift loss coefficient ΔC_L. Current limitations of the proposed method are:

- Only the magnitude of the velocity is scaled, which prevents the modeling of any cross flow induced by the spoiler deflection. In future work, velocity components will be scaled independently
- All spoilers are modelled using the same smooth functions, which prevents the possibility of having spoilers deflected at different angles, i.e. generating different local variation of the lift coefficient
- The whole region behind the spoiler is modelled with the same smooth function, which prevents the ability of

modeling flow reattachment for small spoiler deflection angles.

Results show good agreement with the experimental data and show the ability of the low-fidelity aerodynamic solver to provide a good estimation of the full nonlinear region behind the deflected spoiler.

Acknowledgments

This work was funded by the Engineering and Physical Sciences Research Council (EPSRC) in the UK within the project "Experimental Flight Dynamics Testing for Highly Flexible Aircraft", ref. no. EP/T018739/1. The authors would also like to thank Dr Xiao Liu and Luke Bowen for their valued support during the PIV test campaign.

References

[1] Abbas, A., De Vicente, J., and Valero, E., "Aerodynamic technologies to improve aircraft performance," *Aerospace Science and Technology*, Vol. 28, No. 1, 2013, pp. 100–132.

[2] Bradley K., M., and Droney K., C., "Subsonic Ultra Green Aircraft Research Phase II: N+4 Advanced Concept Development," Tech. rep., 2012.

[3] Bradley, M. K., and Droney, C. K., "Subsonic Ultra Green Aircraft Research: Phase I," Tech. Rep. April, 2011.

[4] Collar, A. R., "The expanding domain of aeroelasticity," *The Royal Aeronautic Society*, 1946.

[5] Dussart, G., Portapas, V., Pontillo, A., and Lone, M. M., "Flight Dynamic Modelling and Simulation of Large Flexible Aircraft," *Flight Physics - Models, Techniques and Technologies*, 2018.

[6] ESDU, "ESDU 14004 - Lift and rolling moment due to spoilers on wings at subsonic speeds with trailing-edge flaps undeployed," *ESDU Series on Aerodynamics*, , No. November, 2014.

[7] ESDU, "ESDU 96026c - Drag and yawing moment due to spoilers," *ESDU Series on Aerodynamics*, , No. November, 2014.

[8] Mack, M. D., Seetharam, H. C., Kuhn, W. G., and Bright, J. T., "Aerodynamics of spoiler control devices," *AIAA-79-1873*, 1979.

[9] Roskam, J., and Kohlman, D. L., "Spoilers for roll control of light airplanes," *AIAA-74-861*, 1974.

[10] Costes, M., "Comparison between experimental and computational results for airfoils equipped with a spoiler and a flap," *AIAA-85-5008*, 1985.

[11] Wentz, W. H., Ostowari, C., and Seetharam, H. C., "Effects of Design Variables on Spoiler Control Effectiveness, Hinge Moments and Wake Turbulence." *AIAA-81-0072*, 1981.

[12] Pontillo, A., Navaratna, P. D. B., Ascham, J., Lowenberg, M. H., Rezgui, D., Cooper, J. E., and Neild, S. A., *Low-order Aeroelastic Modelling of a High Aspect Ratio Wing Aircraft Under Constrained Motion*, AIAA SCITECH 2022 Forum, 2022.

[13] Navaratna, P. D. B., Pontillo, A., Rezgui, D., Lowenberg, M. H., Neild, S. A., and Cooper, J. E., *Numerical Investigations of Subscale Flexible High Aspect Ratio Aircraft on a Dynamic Wind Tunnel Rig*, AIAA SCITECH 2023 Forum, 2023.

[14] Katz, J., and Plotkin, A., *Low-Speed Aerodynamics*, 2nd ed., Cambridge University Press, New York, 2001.

[15] Barrett, R., "Design and performance of a new low turbulence wind tunnel at Bristol University," *The Aeronautical Journal (1968)*, Vol. 88, No. 873, 1984, p. 86–90. https://doi.org/10.1017/S000192400002025X.